Osteoarthritis Cartilage. Author manuscript; available in PMC 2016 November 30.

Published in final edited form as:

Osteoarthritis Cartilage. 2008 April ; 16(4): 458–469. doi:10.1016/j.joca.2007.08.006.

Study of subchondral bone adaptations in a rodent surgical model of OA using *in vivo* micro-computed tomography[1]

D. D. McErlain, M.Sc.[†,‡,*], **C. T. G. Appleton, Ph.D.**[§], **R. B. Litchfield, M.D., F.R.C.S.(C).**[‖], **V. Pitelka, Ph.D.**[§], **J. L. Henry, Ph.D.**[¶], **S. M. Bernier, Ph.D.**[#,a], **F. Beier, Ph.D.**[§], and **D. W. Holdsworth, Ph.D.**[†,‡,††]

[†]Imaging Research Laboratories, Robarts Research Institute, University of Western Ontario, London, Canada

[‡]Department of Medical Biophysics, University of Western Ontario, London, Canada

[§]Department of Physiology and Pharmacology, University of Western Ontario, London, Canada

[‖]Fowler Kennedy Sport Medicine Clinic, University of Western Ontario, London, Canada

[¶]Michael G. DeGroote Institute for Pain Research and Care, Department of Psychiatry, Behavioural Neurosciences and Anaesthesia, McMaster University, Hamilton, Canada

[#]Department of Anatomy and Cell Biology, University of Western Ontario, London, Canada

[††]Department of Diagnostic Radiology and Nuclear Medicine, University of Western Ontario, London, Canada

Summary

Objective—To non-invasively investigate the changes to epiphyseal bone occurring in a longitudinal pre-clinical model of osteoarthritis (OA) using *in vivo* micro-computed tomography (micro-CT).

Design—*In vivo* micro-CT images were acquired using a bench-top micro-CT scanner, which produces three-dimensional data with isotropic voxel spacing of 0.046 mm. Male rodents were scanned prior to surgical destabilization, consisting of anterior cruciate ligament transection and partial medial menisectomy (ACLX). Subsequent scans were performed every 4 weeks post-ACLX, for up to 5 months. Volumetric bone mineral density (vBMD) was measured in specific, anatomically segmented regions within each image. The ACLX rodent data were compared with the contralateral non-operated hind limb of the same animal, as well as a sham-operated group (SHAM) of animals, for each time point. End-point histology compared changes to cartilage and bone between the ACLX and control animals.

[1]This study was funded as part of the Canadian Institutes of Health Research (CIHR) Operating Grant 67018, the New Emerging Team grant provided by the CIHR and the Canadian Arthritis Network, and the Ontario Research and Development Challenge Fund. D. W. Holdsworth is a Career Investigator, supported by the Heart and Stroke Foundation of Ontario.

[*]Address correspondence and reprint requests to: D. D. McErlain, Department of Medical Biophysics, University of Western Ontario, London, Canada. dmcerl@imaging.robarts.ca.

[a]Deceased May 3, 2007.

Results—The micro-CT protocol produced sufficient spatial resolution and signal-to-noise ratio (SNR = 19) to quantify subchondral bone pathology, with an acceptable entrance exposure to radiation (0.36 Gy). Significantly lower vBMD was measured in the ACLX group, vs SHAM rodents, at 1, 4, and 5 months post-surgery ($P < 0.05$). Qualitative observations of ACLX joints revealed significant loss of cartilage, subchondral bone cysts, and calcification of tendon similar to changes found in humans.

Conclusions—This study demonstrates *in vivo* micro-CT as an effective method for investigating the development of rodent knee OA longitudinally. This method can be applied, in future pre-clinical trials, to non-destructively monitor the efficacy of pharmacological interventions.

Keywords

Osteoarthritis; Micro-computed tomography; Rodent; Knee joint; Subchondral bone; Bone mineral density

Introduction

Osteoarthritis (OA) is a degenerative disease, having a complex etiopathology[1–3], affecting both the articular cartilage and underlying subchondral bone within synovial joints[4,5]. OA is the most prevalent form of arthritis[6], and contributes significant economical and social impacts to the patient, the health care system, and the labour force in Canada[7]. With the advent of an aging population, OA is projected to affect an increasing number of Canadians[8], which is driving the demand for disease-modifying OA drugs (DMOADs) to treat the functional deficits, along with the symptoms. It is therefore of critical importance to adopt a pre-clinical model of OA that is reproducible and can be used to investigate the mechanisms of this disease, with the hopes of studying pharmacological interventions longitudinally.

Before clinical trials of a new drug can begin, investigations are carried out in animal models that produce human-like OA characteristics[9–11]. Most animal-model studies use large species, such as cows[11], sheep[12], or dogs[13] in order to obtain sufficient amounts of tissue for histological or histomorphometric analyses. However, the housing and animal-care costs associated with larger animals may limit the number of samples used for longitudinal investigations of joint degeneration. To offset animal-care costs, many investigators have chosen smaller species, including rabbits[14,15], guinea pigs[16], and rodents[17] to examine the initiation and progression of OA. Rodents are of particular interest (with well-established genomes) in the areas of research determining the genetic links or changes in expression that occur in OA[18,19]. The rat specifically is an ideal animal model for longitudinal, *in vivo* research due to their ease of handling and housing, and their ability to support surgical[20] and adjuvant induced[21] OA.

Improvements in non-destructive imaging modalities such as magnetic resonance imaging (MRI) and computed tomography (CT) allow investigators to create images of the three-dimensional (3D) architecture of joints in humans with OA[22]. However, two-dimensional (2D) radiographs are still the clinical standard for humans[23], though recent studies suggest

difficulties in consistently grading radiographs, and correlating the grade to pain and joint function[23,24]. MRI has been identified as the preferred tool for future clinical trials[25] but it is limited to using larger animals in pre-clinical trials due to insufficient spatial resolution. Increasing the field strength can offset this disadvantage and improve the signal-to-noise ratio (SNR)[26], but the length of scan time needed to acquire these images with sufficient spatial resolution makes *in vivo* data acquisition exceedingly difficult. Most investigators have used *ex vivo* MRI analyses with dogs[27], rabbits[15], or guinea pigs[28] to obtain excellent cartilage and bone images, while those performing *in vivo* experiments use rabbits and guinea pigs with some form of contrast agent to enhance visualization of soft tissue[29]. Recently, micro-computed tomography (micro-CT) systems have become available that can provide superior spatial resolution and contrast between bone and soft tissue, when compared to clinical CT. Most systems implement micro-focus X-ray tubes combined with megapixel charge-coupled device (CCD) detectors to create very high-resolution images with varying isotropic voxel sizes from 10 to 100 microns (μm)[30,31]. The use of these systems is quickly becoming a standard reference tool for the pre-clinical and non-destructive analysis of bone density, stereology or architecture in small animals[31,32] and bone specimens[33,34].

Our previous experience using non-invasive micro-CT and high-field MRI imaging with a rabbit model of OA accurately portrayed progressive changes to cartilage, the volumetric bone mineral density (vBMD), and the development of osteophytes in the knee[14,15]. However, this analysis was performed *ex vivo*, requiring animal euthanasia at each desired interval. Concurrent advances in non-invasive micro-CT imaging can now allow *in vivo* imaging of small-animal joints with isotropic resolution between 25 and 100 μm[35,36] in as little as 10 min. Thus, the purpose of this study was to incorporate this new technology with a more cost-effective, longitudinal animal model of OA. We have accomplished this purpose by using a surgical destabilization model in the rodent knee. It is our belief that *in vivo* micro-CT imaging, when applied to a rodent anterior cruciate ligament transection with partial menisectomy (ACLX) model, accurately characterizes the changes to subchondral bone in human-like OA development. In this longitudinal study over a 5-month period, we were able to accurately quantify the changes to vBMD and joint derangement in the same animal during the initiation, progression, and end stages (or joint failure) of OA development. This validation study sets the precedent for future investigations into possible treatments or pharmacological interventions using our non-invasive and longitudinal model.

Materials and methods

ANIMAL MODEL

All the animals used in this study were healthy, male Sprague–Dawley rats obtained from Charles River Inc. (St. Constant, QC, Canada). At approximately 3 weeks of age, 18 rats (mean body weight 301 ± 13 g) were randomly assigned into either the experimental or the control group. Surgical procedures were performed on the right hind limb only. Fifteen rats underwent transection of the anterior cruciate ligament with partial medial menis-cectomy (ACLX). The non-operated, or left hind limbs of the ACLX animals (LEFT) were used as a control group throughout the experiment, while the three remaining rats were randomly

assigned to a sham-operated group (SHAM), to control for the effects of the surgery. The Animal Use Subcommittee of the University of Western Ontario approved all animal manipulations. Animals were monitored on a daily basis and, before any experiment, their body weights were measured. Between imaging experiments, all animals were housed in standard cages and permitted free activity with food and water *ad libitum*.

All animals were deeply anaesthetized with a mixture of ketamine (100 mg/ml), xylazine (5 mg/ml) and saline. The dose was maintained at 0.1 ml per 100 g of body weight throughout all surgical and imaging experiments. After administering anesthetic, the rodents were given 0.1 ml per 100 g of body weight of the antibiotic Trisbrissen 24% (Schering Canada Inc., Pointe Claire, QC, Canada). An incision measuring approximately 1 cm was made medial to the patella, allowing displacement of the patella with the hind limb extended. The knee was subsequently flexed and, with a bent 27-gage needle, the medial meniscus was hooked and pulled gently away from the tibial plateau. The synovial and tibial attachments of the meniscus were visualized and severed using a pair of dura scissors. Once the medial meniscus was removed, and the anterior cruciate ligament (ACL) was visualized, the same bent needle was used to hook the ligament and sever it. Rigorous precautions were employed to avoid damage to articular surfaces, which were kept moist throughout the procedure with sterile saline. Once the procedure was complete, the incision was sutured in two layers. In SHAM, the procedure was similar to the ACLX surgery. However, upon hooking and gently pulling the medial meniscus away from the tibial plateau, the incision was sutured in two layers. All ACLX and SHAM animals were observed and neither appeared to favor the operated leg upon recovery from anesthesia, nor at any time point afterward.

The hind limbs of all animals were imaged with micro-CT on the day prior to surgical intervention and every 4 weeks post-surgery for up to 20 weeks (six time points). In the ACLX group, three animals were euthanized ($n = 3$) at each time point with an overdose of anesthetic following micro-CT imaging, for use in another study.

MICRO-CT PROTOCOL

In vivo micro-CT imaging was performed using a bench-top micro-CT scanner (Locus, GEHC, London, ON, Canada) scanner. The imaging protocol was optimized over multiple pilot scans, using an excised rat knee stored in formalin in a 50 ml tube, before any live animal scans were performed. The X-ray tube has a tungsten target, with a nominal spot size of 50 μm, and 1.8 mm Al-equivalent filtration. The protocol was designed so that X-ray projection views were acquired in 1° increments over 210°. These projection images were the summation of five X-ray projections (each projection, acquired over 400 ms at 80 kVp and 0.45 mA) that were averaged at each angular increment to create one image. All acquisition images were subsequently corrected with bright (i.e., X-ray image with nothing in the field of view [FOV]) and dark (i.e., image acquired without X-rays) field images. Finally, the data were then reconstructed using a modified Feldkamp cone-beam reconstruction algorithm[37], resulting in a full 3D micro-CT volume with isotropic voxel spacing of 46 × 46 × 46 μm. The micro-CT volume was calibrated in the conventional linear scale of CT numbers, otherwise known as Hounsfield units (HU), wherein the values for

water and air are 0 and −1000, respectively. The entire time needed to acquire this micro-CT volume was approximately 17 min.

Prior to scanning, the rodents were anaesthetized with the same ketamine–xylazine mixture described above. The animal was placed in the supine position and a tissue calibration phantom was attached to the operated leg, which was splinted to prevent any motion during the scan. The phantom was made of a 1 mm diameter cylinder of an epoxy-based material that is known to mimic the radiographic properties of cortical bone (SB3, Gamex RMI, Middleton, USA)[38] [Fig. 1(b)]. The animal was subsequently placed on a carbon fiber bed [Fig. 1(a)] that transported the animal into the bore of the scanner. The 65 mm FOV provided by the micro-CT system allows the simultaneous imaging of both hind limbs in one acquisition [Fig. 1(b)]. Both operated (ACLX) and contralateral (LEFT) limbs were imaged simultaneously with micro-CT, allowing the investigation of possible systemic effects after the surgery[39,40].

The image quality was quantitatively measured by determining the SNR within the 3D micro-CT volume. This was achieved by placing a square region of interest (ROI) into two selected areas: a region identified as cortical bone and an area of background material.

The SNR was defined as:

$$\mathrm{SNR}=HU_{\mathrm{bone}}/\sigma_{\mathrm{background}}$$

where HU_{bone} is the mean CT number in the cortical bone calibrator, and $\sigma_{background}$ is the standard deviation (SD) within the image background.

Radiation dose—The entrance exposure rate was measured using a 15 cm^3 ion chamber (Model 96035, Keithley, Cleveland, USA) and electrometer (model 617, Keith-ley, Cleveland, USA). It was found to be 190 mR/mAs at the isocentre, and was used to estimate a total entrance X-ray dose of 0.36 Gy per micro-CT volume acquisition. Dare *et al.*[41] reported that single X-ray dose of up to 0.40 Gy did not affect cell growth and proliferation of osteoblast-like cells *in vitro*. A single X-ray dose of 5 Gy can affect osteoblasts in the tibial epiphysis[42], however, our protocol exposed the ACLX and SHAM rodents to a maximum total exposure of only 1.8 Gy over a period of 20 weeks. Allowing adequate time for the rodents to recover from repeated irradiation reduces the chance of radiation-induced damage to the joint. For lower body irradiation, the recovery rate is approximately 33% of the lethal dose – approximately 5–7 Gy whole body exposure for rats[43,44] – per day[45]. Therefore, allowing 4 weeks between micro-CT scans provides an adequate period for the animal to recover from any possible effects of radiation.

HISTOLOGICAL ANALYSIS

At 5 months, the ACLX ($n = 3$), LEFT ($n = 3$), and SHAM rats ($n = 3$) were euthanized by means of intracardial perfusion with 4% paraformaldehyde. Both hind limbs were disarticulated and decalcified in 15% EDTA/glycerol (pH = 7.3) for up to 5 weeks. The knee joints were subsequently embedded in paraffin wax and the medial joint compartment was serially sectioned in the sagittal plane. Three sections – each 6 μm thick and 30 μm apart –

located between 270 and 330 μm from the medial joint margin, were stained with Safranin-O/Fast Green[46].

The Osteoarthritis Research Society International (OARSI) scoring method[46] was used to grade and stage OA degradation in SHAM, LEFT, and ACLX medial knee joint compartments at 5 months in order to quantitatively assess subchondral bone degradation in addition to cartilage. The grade and stage of both joint surfaces was determined, for three slides within each knee joint, by a blinded observer. The OA score was calculated by multiplication of the grade and stage values for each slide. A minimum score of 0 represents no OA degradation and a maximum score of 24 represents the highest degree of OA degradation in more than 50% of the section. Severe characteristics of OA degradation assessed included cartilage denudation, subchondral plate fracture, and evidence of bone repair. The score for each medial compartment joint surface was assigned by determining the average score of all slides assessed from that sample. The score from both surfaces of each joint was then averaged to achieve an OA score representing OA degradation of the whole joint.

IN VIVO BONE ANALYSIS

The reconstructed micro-CT volumes were analyzed with 3D viewing software (Microview 2.0.1; GE Biosciences, London, ON, Canada) as a multi-planar reformatted image (MPR), allowing simultaneous examination of all three planes (axial, coronal, and sagittal). All images were qualitatively viewed in the sagittal and coronal planes for signs of joint degradation, and development of OA, such as the presence of subchondral sclerosis, osteophytes, soft tissue calcifications, and bone cysts or edema.

vBMD—To ensure the accuracy and reproducibility of measuring parameters such as vBMD, a consistent and reliable spatial sampling method was developed initially for the use in human CT studies. This method was later adapted for use with an *ex vivo* micro-CT-rabbit ACLX model by Batiste *et al.*[14,15]. The knee joint was divided into four compartments (medial femur (MFC), lateral femur (LFC), medial tibia (MTP), and lateral tibia (LTP)), each containing anterior, central, and posterior cylindrical ROIs, providing a total of 12 sampling locations (equivalent to ‘‘virtual biopsy’’ sites) per knee joint, as shown in Fig. 2. The weight-bearing regions of both the femur and tibia were used to find the most anterior and posterior margins, thus creating a primary axis, *Y*. Then, the most medial and lateral margins of the compartment were identified to create the secondary axis, *X*. Using these axes, a 2 × 4 grid was created where the primary axis is divided into quarters (*Y*/4) and the secondary axis in half (*X*/2). The central ROI coordinates were defined as the intersection between *Y*/2 and *X*/2; the coordinates for the anterior and posterior ROIs require adjusting for anatomical variation. To accommodate for the natural curvature of the bones, the medial and lateral borders of the anterior and posterior ROIs were determined by the bone–tissue interface along the lines *Y*/4 and *Y*3/4, respectively. Careful attention ensured that the anterior margin in the femur did neither include the patellofemoral region, nor did the anterior margin in the tibia include the tibial tuberosity; thereby maintaining the use of weight-bearing regions of the joint exclusively when calculating the quantitative bone parameters. The minimum distance between the subchondral plate and the epiphyseal plate

(as viewed in the coronal plane) determined the *Z* position, or depth of the ROI; this distance varied between the femur and tibia. Finally, cylindrical ROIs with a diameter of 0.75 mm were placed in the six femoral and in the six tibial subchondral regions, with depths of 1.5 and 0.85 mm, respectively. These ROIs taken from specific, weight-bearing compartments were composed of the subchondral bone plate and the underlying epiphyseal trabecular bone.

STATISTICAL ANALYSIS

The vBMD was tabulated for all 12 anatomical locations within each animal. The anterior, central, and posterior regions within each compartment were averaged to create four compartment means: MFC, LFC, MTP, and LTP[14]. Compartmental vBMD within each group (ACLX, SHAM, and LEFT) was examined using a one-way repeated-measures analysis of variance (ANOVA), with a Tukey HSD multiple-comparison *post hoc* test to identify any significant relationships between time points. Paired *t* tests were implemented to assess the change to compartmental vBMD during the experiment between the ACLX and SHAM groups, and between the ACLX and LEFT groups in each compartment at every time point. Differences were considered significant for $P < 0.05$. All statistical analyses were performed using Prism v4.0a, GraphPad Software Inc. (San Diego, CA, USA).

Results

IMAGE QUALITY

The *in vivo* micro-CT protocol gave an SNR of 19, at an entrance dose of 0.36 Gy. This *in vivo* micro-CT protocol provided sufficient spatial resolution for qualitative visualization of the structure and morphology in subchondral bone. Comparable assessments of signs of joint degradation and demineralization, such as changes to trabecular morphology, could be achieved with the use of an *ex vivo* protocol with a higher entrance dose.

QUANTITATIVE CHANGES TO OA JOINTS

Values reported within the three ROIs (anterior, central, and posterior) in each compartment (LFC, MFC, LTP, and MTP) were averaged, producing a single compartment mean[14]. For all rodents in each group, the femoral ROIs were composed of approximately5670voxels, witha corresponding volume of 0.60 μl. The number of voxels and corresponding volume in the tibial ROIs were 3270 and 0.35 μl, respectively. Repeated-measures ANOVA revealed that the main effect of time post-surgery was significant for each compartmental vBMD for all groups ($P < 0.001$). Summaries of the descriptive statistics for all groups are provided in Table I.

Measurement of vBMD between surgical groups—The difference in vBMD from pre-surgical determination was calculated and plotted in Fig. 3. The vBMD data consisting of the rat knees used throughout the entire experiment ($n = 3$ for each group) is plotted in Fig. 4. Paired *t* tests revealed that the vBMD values for knees in the pre-surgical LEFT group were unexpectedly greater than vBMD values for pre-surgical SHAM knees ($P < 0.05$); no other significant differences between the LEFT and SHAM groups were found at any other time point. The vBMD in SHAM knees was also lower than the vBMD in ACLX

(i.e., right) knees prior to surgery, although it should be noted that, pre-surgical values obtained in the SHAM group were on average within 45 mg cm^{-3} (8%) of both the ACLX and LEFT limbs. All pre-surgical rat knees scanned exhibited a wider epiphyseal growth plate than observed at all time points post-surgery. Immediately 1 month after surgery, however, the SHAM and LEFT groups exhibited significantly higher vBMD than the ACLX limb ($P < 0.01$). No significant differences in vBMD were found again until 4 months after surgery, at which point the SHAM and LEFT limbs were significantly higher than the ACLX group ($P < 0.01$ and $P < 0.05$, respectively). The ACLX animals exhibited an overall decrease of 6.3% (41 mg cm^{-3}) in vBMD at 4 months. There was a 9% (55 mg cm^{-3}) overall increase in vBMD, from 4 to 5 months by the ACLX group, though still significantly lower than the vBMD in both SHAM and LEFT groups.

Longitudinal changes to vBMD—Within both femoral compartments, the LFC and MFC, Tukey *post hoc* tests revealed that the vBMD within the ACLX rats was significantly higher at all time points post-ACLX than their pre-surgical (pre-ACLX) measurement ($P < 0.001$). The only other significant difference observed along time points post-ACLX was between 1 and 2 months; where there was a vBMD increase of 13.7% (85 mg cm^{-3}) in the LFC ($P < 0.01$), and 16.3% (95 mg cm^{-3}) in the MFC vBMD ($P < 0.001$). In the femoral compartments for both the LEFT and SHAM knees, the only significant differences in vBMD were found between all post-intervention time points vs values determined pre-intervention ($P < 0.05$ and $P < 0.01$, for the LEFT and SHAM femoral compartments, respectively).

The LTP in the ACLX group was the only compartment in which the 1 month post-ACLX vBMD was not significantly higher than pre-ACLX ($P > 0.05$). The vBMD of both the LTP and MTP of the ACLX decreased from 3 to 4 months post-ACLX by 5.9% (36 mg cm^{-3}) and 5.2% (34 mg cm^{-3}), respectively. Four months post-ACLX, the vBMD in the tibia was not significantly higher than the pre-ACLX values ($P > 0.05$) in each compartment. Subsequently, at 5 months post-ACLX, the vBMD in the LTP and MTP increased significantly higher again than pre-ACLX ($P < 0.05$ and $P < 0.01$, respectively). However, the only significant difference observed between post-ACLX vBMD in the tibia occurred between 1 and 2 months ($P < 0.05$). The pattern for compartmental vBMD within the femur of SHAM animals was duplicated in their LTP and MTP compartments; demonstrating a significantly higher vBMD ($P < 0.05$ and $P < 0.01$, respectively) in all post-SHAM time points vs the pre-SHAM. The LEFT LTP compartmental vBMD exhibited a similar trend to the LTP of the ACLX group, although the decrease in vBMD at 4 months was still significantly higher than pre-LEFT ($P < 0.05$). Upon reaching 5 months, the vBMD in both tibial compartments of the LEFT group increased by 13.1% (82 mg cm^{-3}) in the LTP, and 11.8% (86 mg cm^{-3}) in the MTP, although not significantly higher than any of the post-LEFT values.

Cartilage degradation—Examination of the *in vivo* sagittal micro-CT images of the medial joints at 5 months revealed superficial damage to the subchondral bone, as evidenced by sclerosis and thickening of the subchondral plate of both the femur and tibia of the ACLX joints [Fig. 5(a)] compared to LEFT [Fig. 5(b)] and SHAM (not shown) joints. These joints

were fixed, decalcified and subjected to histological analysis with Safranin-O and Fast Green staining. Almost all of the articular cartilage was eroded from the femur and tibia of ACLX animals [Fig. 5(c)], whereas a fully intact joint surface with evenly distributed chondrocytes was observed in the hind limbs of SHAM and LEFT animals [Fig. 5(d)]. Upon closer inspection of the ACLX tissue, we found areas where the subchondral bone was invaded with cartilaginous and other fibrous tissue [Fig. 5(c)] suggesting that remodeling processes were being carried out within the OA joint. The mean OARSI score of the 5-month ACLX hind limbs (19.8 ± 1.7) was significantly higher than both the SHAM and LEFT groups ($P < 0.01$, Table I). While no significant difference was found between the control groups (0.3 ± 0.3 and 1.6 ± 1.3, respectively).

QUALITATIVE CHANGES TO OA JOINTS

Bone cyst formation—Qualitative investigation of the medial knee joint from the coronal view of the micro-CT images revealed radiolucent areas in both the MFC and MTP, as shown in Fig. 6. Within the MTP, the small focal areas of bone resorption appeared in the weight-bearing regions of 92% of the knees ($n = 11$) at 2 months post-ACLX. These areas are consistent with the formation of subchondral bone cysts. There was a noticeable breach of the subchondral plate associated with the formation of cysts [Fig. 6(c)]. The subchondral bone cysts appeared to increase, in area as well as number, in all post-ACLX rats throughout the final time points, however, the breach to the subchondral plate appeared to be covered with mature osteoid after 3 months. The subchondral cysts in the posterior aspect of the MFC were more variable in size and rate of appearance. Active sites of resorption appeared further away from the articular surface at 3 months post-ACLX in only 56% of the animals (five out of nine). By 4 months, 83% (five out of six) of ACLX knees showed a loss of mature trabecular bone in the MFC, and at 5 months, all ACLX rodents showed enlarged cyst formation throughout the central and posterior MFC compartments. No cysts or articular surface abnormalities were observed within the LFC or LTP of ACLX animals. No cysts were observed in any compartment of either the SHAM-operated or the LEFT (contralateral) limb at any time points.

Histological analysis of these subchondral cysts (Fig. 7) revealed sites of bone resorption, and a predominance of fibrous tissue deposition surrounding regions consistent with marrow and non-marrow components. The tissue that replaced cancellous bone displayed increased cellularity, coupled to a more disorganized fiber arrangement and density; as evidenced by paler staining than neighboring bone, resembling hyperplastic connective tissue [Fig. 6(d)].

Patellar tendon calcification—Examination of the ACLX knee joints in the sagittal plane directly between the medial and lateral compartments revealed ossification of the patellar tendon (Fig. 8). This developed as small calcifications just inferior to the midsection of all patellae ($n = 12$) 2 months post-ACLX. By the end stage of the experiment, the bone formation demonstrated a cancellous structure in the middle, surrounded by a more dense, cortical bone network indicating heterotopic ossification, a form of the more commonly known myositis ossificans[47]. This patellar tendon calcification appeared in only one (33%) of the SHAM group, after 3 months, and was not found in any of the LEFT hind limbs.

The qualitative analysis of the joints revealed sclerosis of the subchondral plate in all ACLX rats, with some evidence of marginal osteophytes in the LFC. However, the formation of these osteophytes did not appear until the later stages of development in less than one third of the animals. Neither the SHAM nor the LEFT group exhibited any major changes in subchondral plate thickness, surface roughness, or osteophyte formation.

Discussion

The goal of this study was to characterize and validate a quantitative, non-invasive, and longitudinal rodent model of surgically induced OA, using *in vivo* micro-CT to monitor the changes to subchondral bone. This is the first *in vivo* study to examine vBMD over an extended period of time post-ACLX (5 months) in the same animal revealing a significantly lower vBMD in ACLX animals vs non-destabilized controls. The lower vBMD in ACLX animals was found at both the early and late stages of our experiment. The strength of this *in vivo* micro-CT protocol is the ability to conduct a longitudinal study with effective measures of qualitative and quantitative changes to subchondral and trabecular bone within the same rodent without any adverse effects.

IMAGE QUALITY

The SNR and nominal spatial resolution (0.045 mm) provided by the *in vivo* scanner was adequate for determination of regional vBMD in an object as small as the rat hind limb. We chose to characterize vBMD, rather than stereological or architectural parameters (such as trabecular thickness, bone-volume fraction, or structural model index)[48,49], due to the fact that vBMD is less dependent on spatial resolution and therefore more precise in detecting and monitoring changes to subchondral, and underlying trabecular bone in a rodent model of ACLX[14]. Stereological parameters require grey-scale segmentation of an image, based on a selected threshold, making them sensitive to partial-volume effects that are inherent in CT of small structures[50]. A recent study using porcine bones found that small changes in threshold values can lead to much greater differences in bone-volume fraction (BV/ TV)[51]. In humans, it has been proposed that the spatial resolution must be at least 0.175 mm in order to evaluate trabecular bone morphology[52]. Morphological parameters have been used to characterize *ex vivo* rat bones, though these analyses were performed with much higher nominal spatial resolution (as small as 0.006 mm)[53]. Although such high-spatial resolution micro-CT scans are possible, the X-ray dose to the animal and scan time would increase significantly[30], precluding routine *in vivo* application.

LONGITUDINAL vBMD

The values for vBMD increased significantly post-intervention in all three groups. This indicates that the animals used were not skeletally mature prior to the start of the study, as suggested by the wider epiphyseal growth plate seen pre-surgically vs other time points (Fig. 6). All rats were weighed before proceeding with surgery, however, DeMoss and Wright found that mature skeletal development was only partially related to body mass[54]. Therefore, using body mass to determine skeletal maturity, although often used[55], is not a reliable estimate. The screening of epiphyseal growth plates with micro-CT scanning could be used

in future investigations to ascertain the skeletal maturity of the animals before surgery, regardless of body weight[56].

Studies in humans indicate that BMD increases in OA patients, compared to the normal population[57,58]. However, data from 3D dual energy X-ray absorptiometry (DEXA) analysis found a decrease in vBMD with early signs of OA[59]. Buckland-Wright identified that even with subchondral plate sclerosis seen in radiographs at advanced stages of OA, there is a loss of mature bone matrix immediately beneath the subchondral plate[60]. The quality of bone in this thickened subchondral plate was found to be less stiff, containing lower amounts of bone mineral with altered matrix properties compared to non-OA bone[61]. This non-linear relationship between vBMD and OA was seen in the ACLX hind limbs. The vBMD for the pre-SHAM group was significantly lower than the ACLX and LEFT groups. However, 1 month after surgery the vBMD in both the LEFT and SHAM limbs increased significantly relative to the ACLX limb. OA models using dogs and rabbits consider the time point 1 month after surgical destabilization to represent an early stage of OA development[14,62], in which the vBMD decreases. This early decrease is due to significant bone resorption, and has been observed in dogs[63] and as early as 2 weeks post-ACLX in rats[64]. Our results confirm these findings, as the mechanically destabilized limb had significantly lower vBMD, even after controlling for the effects of surgery.

A strength of the present study is that we extended the analysis in the same rats and could monitor changes to vBMD within a given animal. The ACLX hind limb recovered from the earlier loss of vBMD at 2 and 3 months, which indicates a net increase in bone mass with changes to structural geometry[65]. As described by Burr, the advanced stages of OA are characterized by remodeling of subchondral bone, resulting in decreased density and stiffness. A poor remodeling process, found in the OA rodents at 4 months, showed an approximate 12% loss in vBMD, indicating an increase in bone turnover in the diseased joint[66]. The vBMD values in the tibia specifically, did not differ significantly from the pre-surgical values at 4 months post-ACLX [Fig. 3(c,d)]. The increased bone turnover appeared to be a systemic response, as the LEFT or contra-lateral hind limb showed a mild decrease in LTP vBMD [Fig. 3(c)], although not significant from other time points. Even with a seemingly systemic increase in vBMD 5 months post-ACLX, the OA limb remained significantly lower than the SHAM animals. Studies with durations as long as 54 months[67] found an increased subchondral plate thickness and bone formation, with BMD values significantly higher than those obtained in the early stage OA. Similarly, our study demonstrated an increase in vBMD from 4 to 5 months post-ACLX, within the same animal. Although this increase in vBMD was not statistically significant, our study may have been limited by the smaller sample size at 5 months ACLX ($n = 3$) than at 1 month ACLX ($n = 15$). A retrospective statistical analysis using a two-tailed, unpaired t test indicated that differences of approximately 80 mg cm^{-3} between groups would be considered significant ($P < 0.05$) with $n = 8$ animals and 80% power. However, results amongst our sample size were very consistent as evidenced by the small variability of vBMD data (Table I), and statistically significant differences were detected between groups of equal sample size (Fig. 3).

QUALITATIVE CHANGES TO OA JOINTS

The benefit of observing animals longitudinally – vs multiple specimens at each time point – is a reduction in inter-specimen variability. While investigating the qualitative changes to the ACLX joint, we were able to successfully monitor the initiation and progression of subchondral bone cysts, seen as early as 2 months post-ACLX. Studies using an iodoacetate-induced rodent model report subchondral cysts with subsequent loss of trabecular structure within 3 weeks of OA induction[68]. In human OA, subchondral cysts are believed to arise in weight-bearing regions of joints through two possible mechanisms: synovial intrusion or bony contusion[69,70]. Synovial intrusion is depicted by cartilage degeneration, allowing synovial fluid into subchondral bone through gaps in the subchondral plate. These cysts initially have open communication with the joint until becoming occluded by fibrous tissue[71]. The second mechanism, bony contusion, is also initiated by cartilage degeneration from abnormal stress; the difference occurs when micro-fractures in the trabeculae, coupled with vascular insufficiency for repair, cause cyst formation. Unfortunately, we cannot yet confirm which mechanism best defines the cyst formation in our model until a more detailed histomorphometric analysis is completed. Furthermore, cystic tissue in OA is capable of recruiting and activating higher numbers of osteoclasts in rats[68,72] than non-OA tissue. This would explain the longitudinal expansion of the lesions, seen especially in the MFC of the ACLX hind limb. It should be noted that these animals did not undergo any surgical reconstruction of the knee to prevent further degeneration of the joint over the 5 months post-surgery. In addition, the joint changes found in the rat knee are more severe, and the expansion of cystic tissue was beyond what is normally be seen in human OA[73], or other animal models. OA severity is normally monitored with radiographs in humans[22,74], which neither typically detect disease severity[24,75] nor subchondral cysts well[76]. Therefore, the use of 3D imaging modalities, such as CT, may improve the detection of painful subchondral bone deformations.

The pathological ossification of muscle tendons has been reported in various joints in humans[77,78], and in the knee following traumatic injury[79] or reconstructive surgery[47], causing serious pain and disability. Heterotopic ossification seen in the patellar tendon of all ACLX animals was originally thought to arise from a change in gait pattern caused by the mechanical destabilization. After observing the same ossification in one of three of SHAM animals, we now postulate that it may originate from the retraction of the patella during both surgeries. This retraction causes bleeding from the tendon, which can clot and mineralize into a mature bone structure. Tendon calcification is likely a wound-healing response to surgery, as it was not observed in any contralateral limbs.

This study is the first to use *in vivo* micro-CT technology to monitor and validate a long-term small animal model of secondary OA. Transection of the ACL with medial menisectomy in rodents leads to degenerative changes in subchondral and trabecular bone identical to those seen in humans. The progressive changes to vBMD, subchondral, and trabecular bone after ACLX were significantly different than control groups in early- and late-stage OA, even after controlling for the effect of surgery. *In vivo* micro-CT was able to measure significant changes in vBMD, heterotopic ossification, and subchondral cyst formation within the same animals over time. Simultaneously scanning both hind limbs

identified no significant differences in vBMD for the SHAM-operated and non-operated LEFT group at any time after surgery. Our *in vivo* micro-CT technique has been applied in an independent study of the effect of forced mobilization on the rodent ACLX model of OA[80]. This study provides novel insights into changes occurring in both cartilaginous and bony tissues during the progression of OA, using repeated, non-destructive, analysis over time in the same animal. Micro-CT can be applied in future pre-clinical trials, to non-destructively determine the response to any pharmacological interventions that may influence the bone within articular joints *in vivo*.

Acknowledgments

The authors thank Dr Nancy Ford, Neil Schwartz, Steven Pollmann, and Patrick Granton for excellent technical assistance.

References

1. Altman R, Asch E, Bloch D, Bole G, Borenstein D, Brandt K, et al. Development of criteria for the classification and reporting of osteoarthritis. Classification of osteoarthritis of the knee. Diagnostic and Therapeutic Criteria Committee of the American Rheumatism Association. Arthritis Rheum. 1986; 29(8):1039–49. [PubMed: 3741515]
2. Felson DT, Neogi T. Osteoarthritis: is it a disease of cartilage or of bone? Arthritis Rheum. 2004; 50(2):341–4. [PubMed: 14872473]
3. Mandelbaum B, Waddell D. Etiology and pathophysiology of osteoarthritis. Orthopedics. 2005; 28(2 Suppl):s207–14. [PubMed: 15747608]
4. Buckwalter JA, Martin J. Degenerative joint disease. Clin Symp. 1995; 47(2):1–32. [PubMed: 7554763]
5. Poole AR. An introduction to the pathophysiology of osteoarthritis. Front Biosci. 1999; 4:D662–70. [PubMed: 10525481]
6. Sangha O. Epidemiology of rheumatic diseases. Rheumatology (Oxford). 2000; 39(Suppl 2):3–12.
7. Badley EM. The effect of osteoarthritis on disability and health care use in Canada. J Rheumatol Suppl. 1995; 43:19–22. [PubMed: 7752126]
8. Badley EM, Wang PP. Arthritis and the aging population: projections of arthritis prevalence in Canada 1991 to 2031. J Rheumatol. 1998; 25(1):138–44. [PubMed: 9458217]
9. Boileau C, Martel-Pelletier J, Brunet J, Tardif G, Schrier D, Flory C, et al. Oral treatment with PD-0200347, an alpha2delta ligand, reduces the development of experimental osteoarthritis by inhibiting metalloproteinases and inducible nitric oxide synthase gene expression and synthesis in cartilage chondrocytes. Arthritis Rheum. 2005; 52(2):488–500. [PubMed: 15693013]
10. Ding M, Christian Danielsen C, Hvid I. Effects of hyaluronan on three-dimensional microarchitecture of subchondral bone tissues in guinea pig primary osteoarthrosis. Bone. 2005; 36(3):489–501. [PubMed: 15777671]
11. Homandberg GA, Ummadi V, Kang H. High molecular weight hyaluronan promotes repair of IL-1 beta-damaged cartilage explants from both young and old bovines. Osteoarthritis Cartilage. 2003; 11(3):177–86. [PubMed: 12623289]
12. Armstrong S, Read R, Ghosh P. The effects of intraarticular hyaluronan on cartilage and subchondral bone changes in an ovine model of early osteoarthritis. J Rheumatol. 1994; 21(4): 680–8. [PubMed: 8035393]
13. Matyas JR, Atley L, Ionescu M, Eyre DR, Poole AR. Analysis of cartilage biomarkers in the early phases of canine experimental osteoarthritis. Arthritis Rheum. 2004; 50(2):543–52. [PubMed: 14872497]
14. Batiste DL, Kirkley A, Laverty S, Thain LM, Spouge AR, Gati JS, et al. High-resolution MRI and micro-CT in an *ex vivo* rabbit anterior cruciate ligament transection model of osteoarthritis. Osteoarthritis Cartilage. 2004; 12(8):614–26. [PubMed: 15262241]

15. Batiste DL, Kirkley A, Laverty S, Thain LM, Spouge AR, Holdsworth DW. *Ex vivo* characterization of articular cartilage and bone lesions in a rabbit ACL transection model of osteoarthritis using MRI and mi-cro-CT. Osteoarthritis Cartilage. 2004; 12(12):986–96. [PubMed: 15564066]
16. Sabatini M, Lesur C, Thomas M, Chomel A, Anract P, de Nanteuil G, et al. Effect of inhibition of matrix metalloproteinases on cartilage loss *in vitro* and in a guinea pig model of osteoarthritis. Arthritis Rheum. 2005; 52(1):171–80. [PubMed: 15641085]
17. Hayami T, Pickarski M, Zhuo Y, Wesolowski GA, Rodan GA, Duong le T. Characterization of articular cartilage and subchondral bone changes in the rat anterior cruciate ligament transection and menis-cectomized models of osteoarthritis. Bone. 2006; 38(2):234–43. [PubMed: 16185945]
18. Zemmyo M, Meharra EJ, Kuhn K, Creighton-Achermann L, Lotz M. Accelerated, aging-dependent development of osteoarthritis in alpha1 integrin-deficient mice. Arthritis Rheum. 2003; 48(10):2873–80. [PubMed: 14558093]
19. Arbeit JM, Hirose R. Murine mentors: transgenic and knockout models of surgical disease. Ann Surg. 1999; 229(1):21–40. [PubMed: 9923797]
20. Karahan S, Kincaid SA, Kammermann JR, Wright JC. Evaluation of the rat stifle joint after transection of the cranial cruciate ligament and partial medial meniscectomy. Comp Med. 2001; 51(6):504–12. [PubMed: 11924812]
21. Bendele A, McComb J, Gould T, McAbee T, Sennello G, Chlipala E, et al. Animal models of arthritis: relevance to human disease. Toxicol Pathol. 1999; 27(1):134–42. [PubMed: 10367688]
22. Raynauld JP, Martel-Pelletier J, Berthiaume MJ, Labonte F, Beaudoin G, de Guise JA, et al. Quantitative magnetic resonance imaging evaluation of knee osteoarthritis progression over two years and correlation with clinical symptoms and radiologic changes. Arthritis Rheum. 2004; 50(2):476–87. [PubMed: 14872490]
23. Hochberg MC, Lethbridge-Cejku M, Tobin JD. Bone mineral density and osteoarthritis: data from the Baltimore Longitudinal Study of Aging. Osteoarthritis Cartilage. 2004; 12(Suppl A):S45–8. [PubMed: 14698641]
24. Barker K, Lamb SE, Toye F, Jackson S, Barrington S. Association between radiographic joint space narrowing, function, pain and muscle power in severe osteoarthritis of the knee. Clin Rehabil. 2004; 18(7):793–800. [PubMed: 15573836]
25. Abadie E, Ethgen D, Avouac B, Bouvenot G, Branco J, Bruyere O, et al. Recommendations for the use of new methods to assess the efficacy of disease-modifying drugs in the treatment of osteoarthritis. Osteoarthritis Cartilage. 2004; 12(4):263–8. [PubMed: 15023377]
26. Gati JS, Menon RS, Ugurbil K, Rutt BK. Experimental determination of the BOLD field strength dependence in vessels and tissue. Magn Reson Med. 1997; 38(2):296–302. [PubMed: 9256111]
27. Lahm A, Uhl M, Edlich M, Erggelet C, Haberstroh J, Kreuz PC. An experimental canine model for subchondral lesions of the knee joint. Knee. 2005; 12(1):51–5. [PubMed: 15664878]
28. Watson PJ, Hall LD, Malcolm A, Tyler JA. Degenerative joint disease in the guinea pig. Use of magnetic resonance imaging to monitor progression of bone pathology. Arthritis Rheum. 1996; 39(8):1327–37. [PubMed: 8702441]
29. Tessier JJ, Bowyer J, Brownrigg NJ, Peers IS, Westwood FR, Waterton JC, et al. Characterisation of the guinea pig model of osteoarthritis by *in vivo* three-dimensional magnetic resonance imaging. Osteoarthritis Cartilage. 2003; 11(12):845–53. [PubMed: 14629960]
30. Ford NL, Thornton MM, Holdsworth DW. Fundamental image quality limits for microcomputed tomography in small animals. Med Phys. 2003; 30(11):2869–77. [PubMed: 14655933]
31. Ritman EL. Micro-computed tomography–current status and developments. Annu Rev Biomed Eng. 2004; 6:185–208. [PubMed: 15255767]
32. Paulus MJ, Gleason SS, Easterly ME, Foltz CJ. A review of high-resolution X-ray computed tomography and other imaging modalities for small animal research. Lab Anim (NY). 2001; 30(3): 36–45.
33. McErlain DD, Chhem RK, Bohay RN, Holdsworth DW. Micro-computed tomography of a 500-year-old tooth: technical note. Can Assoc Radiol J. 2004; 55(4):242–5. [PubMed: 15362347]
34. Muller R, Van Campenhout H, Van Damme B, Van Der Perre G, Dequeker J, Hildebrand T, et al. Morphometric analysis of human bone biopsies: a quantitative structural comparison of

histological sections and micro-computed tomography. Bone. 1998; 23(1):59–66. [PubMed: 9662131]

35. Kinney JH, Lane NE, Haupt DL. *In vivo*, three-dimensional microscopy of trabecular bone. J Bone Miner Res. 1995; 10(2):264–70. [PubMed: 7754806]
36. Waarsing JH, Day JS, van der Linden JC, Ederveen AG, Spanjers C, De Clerck N, et al. Detecting and tracking local changes in the tibiae of individual rats: a novel method to analyse longitudinal *in vivo* micro-CT data. Bone. 2004; 34(1):163–9. [PubMed: 14751574]
37. Feldkamp LA, Goldstein SA, Parfitt AM, Jesion G, Kleerekoper M. The direct examination of three-dimensional bone architecture *in vitro* by computed tomography. J Bone Miner Res. 1989; 4(1):3–11. [PubMed: 2718776]
38. White DR. Tissue substitutes in experimental radiation physics. Med Phys. 1978; 5(6):467–79. [PubMed: 366367]
39. Shakoor N, Block JA, Shott S, Case JP. Nonrandom evolution of end-stage osteoarthritis of the lower limbs. Arthritis Rheum. 2002; 46(12):3185–9. [PubMed: 12483722]
40. Celeste C, Ionescu M, Robin Poole A, Laverty S. Repeated intraarticular injections of triamcinolone acetonide alter cartilage matrix metabolism measured by biomarkers in synovial fluid. J Orthop Res. 2005; 23(3):602–10. [PubMed: 15885481]
41. Dare A, Hachisu R, Yamaguchi A, Yokose S, Yoshiki S, Okano T. Effects of ionizing radiation on proliferation and differentiation of oste-oblast-like cells. J Dent Res. 1997; 76(2):658–64. [PubMed: 9062559]
42. Engstrom H, Jansson JO, Engstrom C. Effect of local irradiation on longitudinal bone growth in the rat. A tetracycline labelling investigation. Acta Radiol Oncol. 1983; 22(2):129–33. [PubMed: 6310967]
43. Sato F, Sasaki S, Kawashima N, Chino F. Late effects of whole or partial body x-irradiation on mice: life shortening. Int J Radiat Biol Relat Stud Phys Chem Med. 1981; 39(6):607–15. [PubMed: 6972927]
44. Kallman RF, Kohn HI. Age, growth, and the LD50 of x-rays. Science. 1956; 124(3231):1078. [PubMed: 13380423]
45. Bond VP, Robertson JS. Vertebrate radiobiology (lethal actions and associated effects). Annu Rev Nucl Sci. 1957; 7:135–62. [PubMed: 13498670]
46. Pritzker KP, Gay S, Jimenez SA, Ostergaard K, Pelletier JP, Revell PA, et al. Osteoarthritis cartilage histopathology: grading and staging. Osteoarthritis Cartilage. 2006; 14(1):13–29. [PubMed: 16242352]
47. Gosselin RA, Belzer JP, Contreras DM. Heterotopic ossification of the patellar tendon following intramedullary nailing of the tibia: report on two cases. J Trauma. 1993; 34(1):161–3. [PubMed: 8437187]
48. Ding M, Odgaard A, Hvid I. Accuracy of cancellous bone volume fraction measured by micro-CT scanning. J Biomech. 1999; 32(3):323–6. [PubMed: 10093033]
49. Hildebrand T, Ruegsegger P. Quantification of bone microarchitecture with the structure model index. Comput Methods Biomech Biomed Engin. 1997; 1(1):15–23. [PubMed: 11264794]
50. Kim DG, Christopherson GT, Dong XN, Fyhrie DP, Yeni YN. The effect of microcomputed tomography scanning and reconstruction voxel size on the accuracy of stereological measurements in human cancellous bone. Bone. 2004; 35(6):1375–82. [PubMed: 15589219]
51. Hara T, Tanck E, Homminga J, Huiskes R. The influence of microcomputed tomography threshold variations on the assessment of structural and mechanical trabecular bone properties. Bone. 2002; 31(1):107–9. [PubMed: 12110421]
52. Muller R, Koller B, Hildebrand T, Laib A, Gianolini S, Ruegsegger P. Resolution dependency of microstructural properties of cancellous bone based on three-dimensional mutomography. Technol Health Care. 1996; 4(1):113–9. [PubMed: 8773313]
53. Ito M, Nishida A, Aoyagi K, Uetani M, Hayashi K, Kawase M. Effects of risedronate on trabecular microstructure and biomechanical properties in ovariectomized rat tibia. Osteoporos Int. 2005; 16(9):1042–8. [PubMed: 15711780]
54. DeMoss DL, Wright GL. Sex and strain differences in whole skeletal development in the rat. Calcif Tissue Int. 1998; 62(2):153–7. [PubMed: 9437049]

55. Iwamoto J, Takeda T, Sato Y. Effect of treadmill exercise on bone mass in female rats. Exp Anim. 2005; 54(1):1–6. [PubMed: 15725675]
56. Martin EA, Ritman EL, Turner RT. Time course of epiphyseal growth plate fusion in rat tibiae. Bone. 2003; 32(3):261–7. [PubMed: 12667553]
57. Radin EL, Rose RM. Role of subchondral bone in the initiation and progression of cartilage damage. Clin Orthop Relat Res. 1986; (213):34–40.
58. Hannan MT, Anderson JJ, Zhang Y, Levy D, Felson DT. Bone mineral density and knee osteoarthritis in elderly men and women. The Framingham Study. Arthritis Rheum. 1993; 36(12): 1671–80. [PubMed: 8250986]
59. Karvonen RL, Miller PR, Nelson DA, Granda JL, Fernandez-Madrid F. Periarticular osteoporosis in osteoarthritis of the knee. J Rheumatol. 1998; 25(11):2187–94. [PubMed: 9818663]
60. Buckland-Wright C. Subchondral bone changes in hand and knee osteoarthritis detected by radiography. Osteoarthritis Cartilage. 2004; 12(Suppl A):S10–9. [PubMed: 14698636]
61. Li B, Aspden RM. Mechanical and material properties of the subchondral bone plate from the femoral head of patients with osteoarthritis or osteoporosis. Ann Rheum Dis. 1997; 56:247–54. [PubMed: 9165997]
62. Boyd SK, Muller R, Matyas JR, Wohl GR, Zernicke RF. Early morphometric and anisotropic change in periarticular cancellous bone in a model of experimental knee osteoarthritis quantified using microcomputed tomography. Clin Biomech (Bristol, Avon). 2000; 15(8):624–31.
63. Pelletier JP, Boileau C, Brunet J, Boily M, Lajeunesse D, Reboul P, et al. The inhibition of subchondral bone resorption in the early phase of experimental dog osteoarthritis by licofelone is associated with a reduction in the synthesis of MMP-13 and cathepsin K. Bone. 2004; 34(3):527–38. [PubMed: 15003800]
64. Hayami T, Pickarski M, Wesolowski GA, McLane J, Bone A, Destefano J, et al. The role of subchondral bone remodeling in osteoarthritis: reduction of cartilage degeneration and prevention of osteophyte formation by alendronate in the rat anterior cruciate ligament transection model. Arthritis Rheum. 2004; 50(4):1193–206. [PubMed: 15077302]
65. Burr DB. Anatomy and physiology of the mineralized tissues: role in the pathogenesis of osteoarthrosis. Osteoarthritis Cartilage. 2004; 12(Suppl A):S20–30. [PubMed: 14698637]
66. Burr DB, Schaffler MB. The involvement of subchondral mineralized tissues in osteoarthrosis: quantitative microscopic evidence. Microsc Res Tech. 1997; 37(4):343–57. [PubMed: 9185156]
67. Brandt KD, Myers SL, Burr D, Albrecht M. Osteoarthritic changes in canine articular cartilage, subchondral bone, and synovium fifty-four months after transection of the anterior cruciate ligament. Arthritis Rheum. 1991; 34(12):1560–70. [PubMed: 1747141]
68. Guzman RE, Evans MG, Bove S, Morenko B, Kilgore K. Mono-iodoacetate-induced histologic changes in subchondral bone and articular cartilage of rat femorotibial joints: an animal model of osteoarthritis. Toxicol Pathol. 2003; 31(6):619–24. [PubMed: 14585729]
69. Resnik, D., Kransdorf, M. Degenerative diseases. In: Ross, A., editor. Bone and Joint Imaging. 3. Philadelphia, PA: Elsevier Inc; 2005. p. 356-443.
70. Durr HD, Martin H, Pellengahr C, Schlemmer M, Maier M, Jansson V. The cause of subchondral bone cysts in osteoarthrosis: a finite element analysis. Acta Orthop Scand. 2004; 75(5):554–8. [PubMed: 15513486]
71. Crawford R, Sabokbar A, Wulke A, Murray DW, Athanasou NA. Expansion of an osteoarthritic cyst associated with wear debris: a case report. J Bone Joint Surg Br. 1998; 80(6):990–3. [PubMed: 9853490]
72. von Rechenberg B, Guenther H, McIlwraith CW, Leutenegger C, Frisbie DD, Akens MK, et al. Fibrous tissue of subchondral cystic lesions in horses produce local mediators and neutral metalloproteinases and cause bone resorption *in vitro*. Vet Surg. 2000; 29(5):420–9. [PubMed: 10999456]
73. Carrino JA, Blum J, Parellada JA, Schweitzer ME, Morrison WB. MRI of bone marrow edema-like signal in the pathogenesis of subchondral cysts. Osteoarthritis Cartilage. 2006; 14(10):1081–5. [PubMed: 16806996]

74. Felson DT, Zhang Y, Hannan MT, Naimark A, Weissman BN, Aliabadi P, et al. The incidence and natural history of knee osteoarthritis in the elderly. The Framingham Osteoarthritis Study. Arthritis Rheum. 1995; 38(10):1500–5. [PubMed: 7575700]

75. LaValley MP, McAlindon TE, Chaisson CE, Levy D, Felson DT. The validity of different definitions of radiographic worsening for longitudinal studies of knee osteoarthritis. J Clin Epidemiol. 2001; 54:30. [PubMed: 11165466]

76. Ostlere SJ, Seeger LL, Eckardt JJ. Subchondral cysts of the tibia secondary to osteoarthritis of the knee. Skeletal Radiol. 1990; 19(4):287–9. [PubMed: 2353215]

77. Fenwick S, Harrall R, Hackney R, Bord S, Horner A, Hazleman B, et al. Endochondral ossification in Achilles and patella tendinopathy. Rheumatology (Oxford). 2002; 41(4):474–6. [PubMed: 11961186]

78. Fuselier CO, Tlapek TA, Sowell RD. Heterotrophic ossification (myositis ossificans) in the foot. A case report. J Am Podiatr Med Assoc. 1986; 76(9):524–6. [PubMed: 3761189]

79. Matsumoto H, Kawakubo M, Otani T, Fujikawa K. Extensive post-traumatic ossification of the patellar tendon. A report of two cases. J Bone Joint Surg Br. 1999; 81(1):34–6. [PubMed: 10067998]

80. Appleton CT, McErlain DD, Pitelka V, Schwartz N, Bernier SM, Henry JL, et al. Forced mobilization accelerates pathogenesis: characterization of a preclinical surgical model of osteoarthritis. Arthritis Res Ther. 2007; 9(1):R13. [PubMed: 17284317]

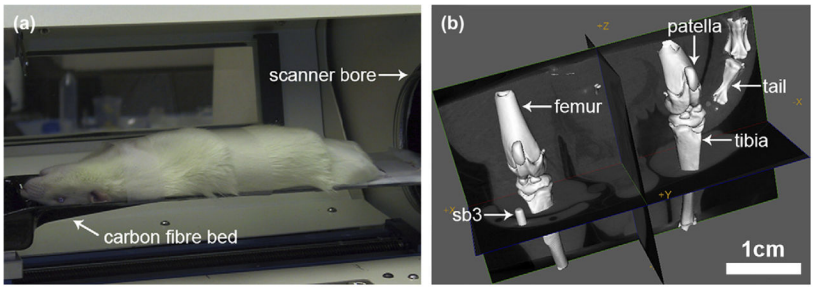

Fig. 1.

In vivo micro-CT imaging of both rodent hind limbs within the FOV provided by the GEHC Locus scanner. (a) Photograph of anaesthetized rodent supine on CT scanner bed. (b) Volume rendering of the CT image produced from our imaging protocol, visualized by GEHC microview.

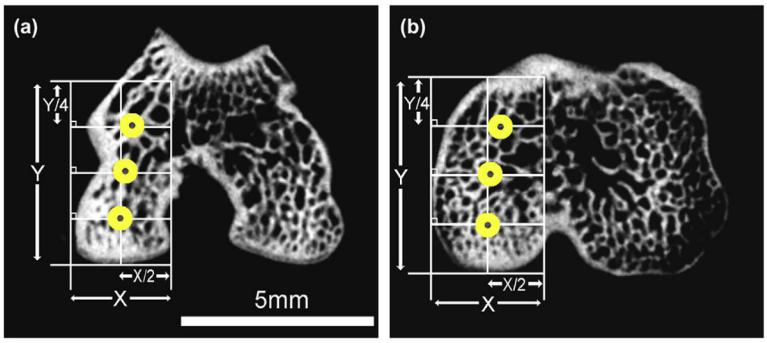

Fig. 2.

Axial plane micro-CT slices displaying the anatomical ROIs as placed in the medial femoral condyle (a) and medial tibial plateau (b).

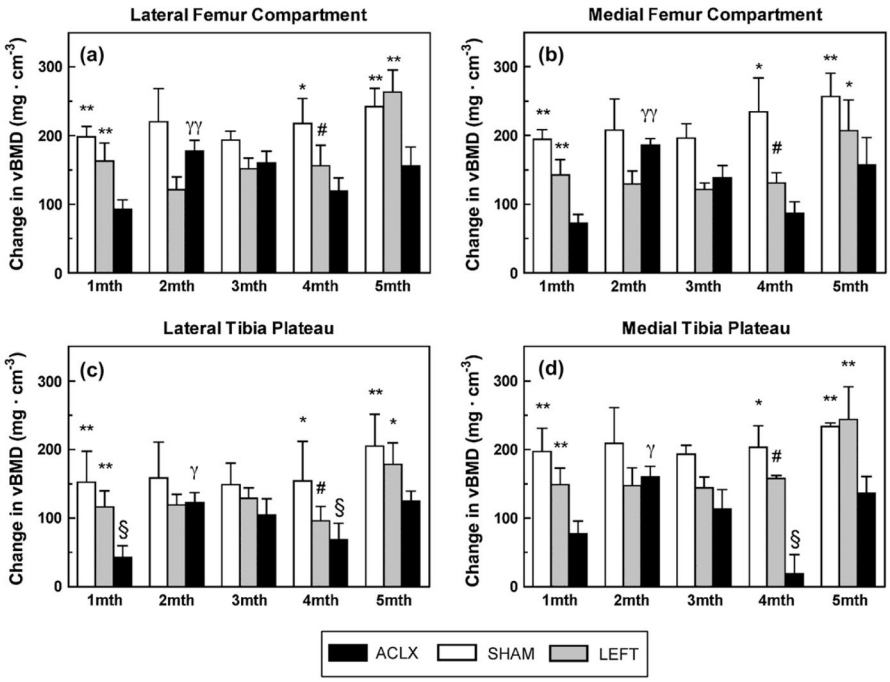

Fig. 3.

Longitudinal changes to vBMD (mean ± S.E.M.) within the four anatomical compartments for all rodents in all surgical groups. *$P < 0.01$ vs ACLX, **$P < 0.001$ vs ACLX, #$P < 0.05$ vs ACLX, $\gamma P < 0.01$ 1 month vs 2 months ACLX, $\gamma\gamma P < 0.001$ 1 month vs 2 month ACLX, §$P > 0.05$ vs pre-surgical vBMD.

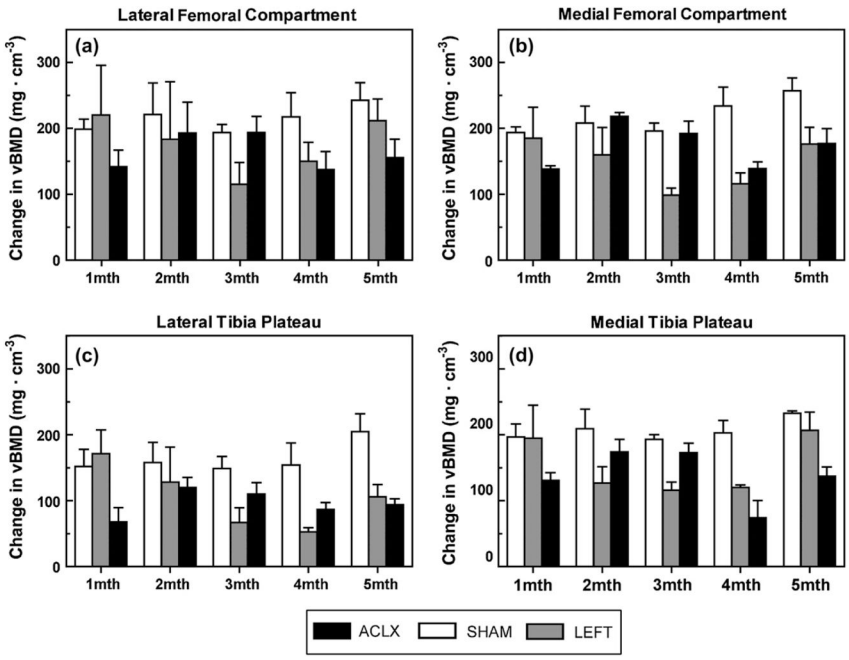

Fig. 4.

Longitudinal *in vivo* vBMD measurements (mean ± S.E.M.) within the (a) LFC, (b) MFC, (c) LTP, and (d) MTP compartments for the rodents imaged at each time point throughout the entire study (ACLX, LEFT, and SHAM groups, $n = 3$).

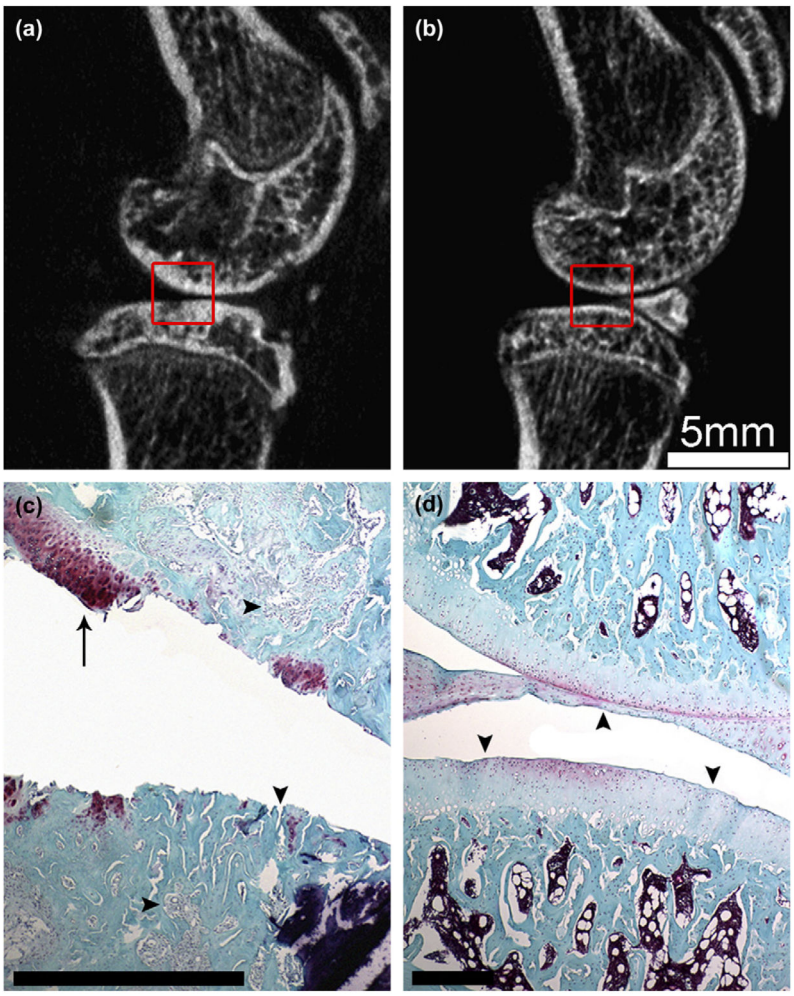

Fig. 5.

Comparison of the tissue changes to the medial joint surfaces. Sagittal *in vivo* micro-CT image of the ACLX (a) and LEFT (b) rodent hind limbs 5 months post-surgery. Note the subchondral plate thickening and loss of mature trabecular bone pattern (a) vs the LEFT limb (b). Joints were fixed, decalcified, and processed for histological staining with Safranin-O and Fast Green. The histological sections were manually registered to the boxed areas of the micro-CT images. Note the delamination of cartilage within the ACLX joint (c), a small remaining tissue fragment (arrow) containing a cluster of chondrocytes. The subchondral bone was invaded at several points (c – vertical arrowhead); while the underlying bony trabeculae were surrounded by fibrous tissue (c – horizontal arrowheads). The cartilage and bone tissue of LEFT limb (d) appeared normal with a consistent, uninterrupted joint surface (arrowheads) and evenly distributed chondrocytes. Scale bar in (c) and (d) = 0.5 mm.

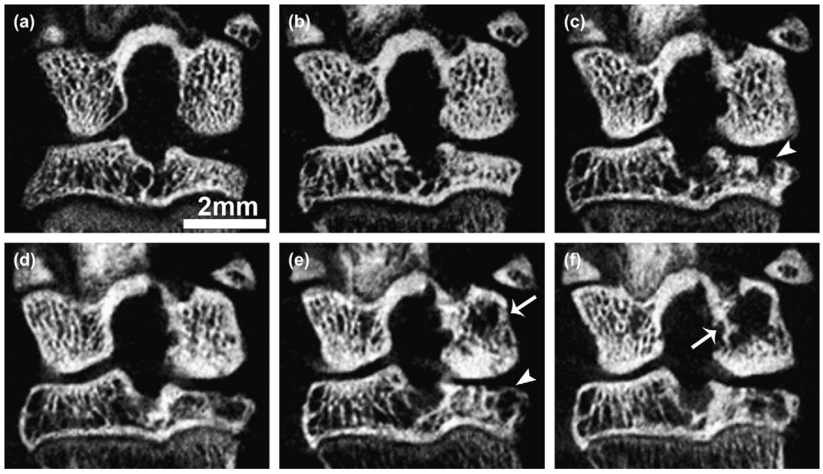

Fig. 6.

Trabecular bone erosion with cyst formation in ACLX knee over time. Coronal *in vivo* micro-CT view at pre-surgical (a), 1 (b), 2 (c), 3 (d), 4 (e), and 5 (f) months post-surgery. Note the breach and eventual covering of the subchondral plate with immature bone (arrowheads), and the increasing area of cysts over time (arrows) within the same animal. These results are representative of findings in all ACLX animals in this study.

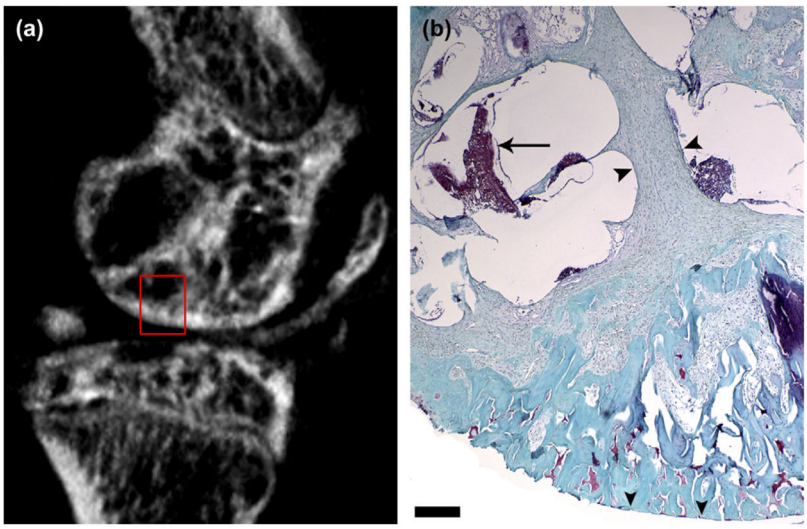

Fig. 7.

Histological analysis of subchondral bone cysts in the medial femoral condyle at 5 months post-ACLX. As predicted by the sagittal micro-CT image (a), there are large cavities under the articular surface (rectangle). Tissue sections of 5 months post-ACLX knee joints were stained with Safranin-O and Fast Green (b). Note the delaminated articular cartilage (vertical arrowheads). The typically expansive sub-chondral bone, as seen in Fig. 4(d), has been replaced with hyperplastic, fibrous tissue (horizontal arrowheads), with some marrow component (arrow). Scale bar = 1 mm.

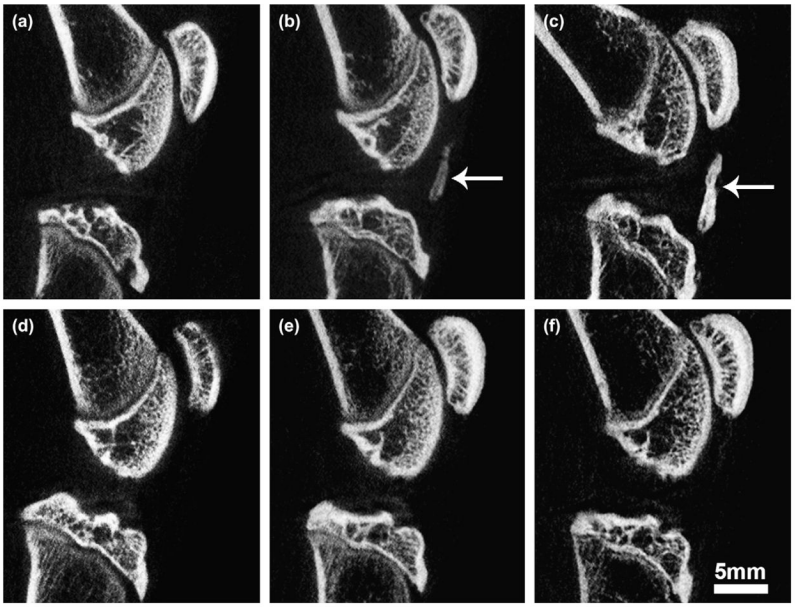

Fig. 8.

Sagittal plane *in vivo* micro-CT images from the mid-line of the joint revealing changes to patellar tendon in the ACLX (a–c) and SHAM (d–f) rodent hind limbs, at 1 month (a,d), 2 months (b,e), and at 5 months (c,f) post-surgery. Note: no calcification in (a), mild calcification in (b) (arrow), with eventual heterotopic ossification at 5 months (arrow, c). Although not seen here, some minor calcification of the tendon was found in one SHAM hind limb.

Table I

Descriptive statistics for compartmental vBMD (mean ± SD), body weight (mean ± SD) in grams, and OARSI score (mean ± SD) for the SHAM, LEFT, and ACLX rodents throughout the course of the experiment. Note the body weights for the ACLX and LEFT groups (both hind limbs of the same rat) are identical. The OARSI score represents the average score for both femoral and tibial joint surfaces

	vBMD (mg cm^{-3})						OARSI score
Compartment	**Pre-surgical**	**1 month**	**2 months**	**3 months**	**4 months**	**5 months**	**5 months**
SHAM	*n* = 3 (292 ± 9 g)	*n* = 3 (383 ± 8 g)	*n* = 3 (424 ± 13 g)	*n* = 3 (490 ± 3 g)	*n* = 3 (549 ± 7 g)	*n* = 3 (596 ± 6 g)	*n* = 3
LFC	502 ± 41	700 ± 52	722 ± 84	695 ± 22	719 ± 63	744 ± 46	0.3 ± 0.3
MFC	463 ± 56	657 ± 24	671 ± 77	659 ± 36	697 ± 86	720 ± 58	
LTP	489 ± 50	641 ± 78	647 ± 91	638 ± 54	643 ± 100	694 ± 81	
MTP	507 ± 64	704 ± 58	716 ± 90	700 ± 23	710 ± 55	740 ± 9	
LEFT	*n* = 15 (310 ± 9 g)	*n* = 15 (409 ± 9 g)	*n* = 12 (463 ± 13 g)	*n* = 9 (519 ± 18 g)	*n* = 6 (579 ± 9 g)	*n* = 3 (622 ± 16 g)	*n* = 3
LFC	533 ± 57	696 ± 101	654 ± 66	685 ± 46	689 ± 74	796 ± 56	1.6 ± 1.3
MFC	543 ± 51	685 ± 88	672 ± 68	664 ± 28	674 ± 37	751 ± 77	
LTP	530 ± 54	646 ± 90	649 ± 52	659 ± 44	626 ± 51	708 ± 55	
MTP	574 ± 54	723 ± 93	721 ± 91	718 ± 48	731 ± 11	818 ± 82	
ACLX	*n* = 15	*n* = 15	*n* = 12	*n* = 9	*n* = 6	*n* = 3	*n* = 3
LFC	528 ± 68	621 ± 52	705 ± 53	688 ± 50	647 ± 47	684 ± 49	19.8 ± 1.7
MFC	511 ± 74	584 ± 49	679 ± 35	650 ± 53	598 ± 42	669 ± 69	
LTP	513 ± 66	556 ± 67	636 ± 51	618 ± 70	582 ± 59	638 ± 26	
MTP	546 ± 69	624 ± 69	706 ± 54	660 ± 84	626 ± 68	683 ± 43	